24th INTERNATIONAL CONGRESS ON SOUND AND VIBRATION
23–27 July 2017, London

ICSV24
23-27JULY 2017
LONDON CALLING

SYNTHESIS OF A SOUND FIELD INCLUDING VIRTUAL SCATTERING OBJECTS IN WAVE FIELD SYNTHESIS

Nara Hahn and Sascha Spors
Institute of Communications Engineering, University of Rostock, Rostock, Germany
email: nara.hahn@uni-rostock.de

In this study, wave field synthesis is used to reproduce a virtual sound field where virtual objects interact with the sound field. These objects do not emit acoustic waves by themselves, but cause reflections and scattering for a given incoming wave. In such a non-freefield scenario, the sound field can be represented as a superposition of the incident field and the scattered field. As proposed by the equivalent source method, a virtual scattering object can be added to a virtual auditory scene by synthesizing a directional sound source and driving it with the source signal of the incident field. The wave field synthesis driving function for the equivalent source is derived by (i) decomposing the scattered field into spherical harmonics up to a finite order, (ii) taking the directional gradient of the sound field at each secondary source position, (iii) and applying a spatial window function to ensure the correct propagation direction within the listening area. The focus of this paper is the creation of the acoustic shadow caused by the destructive interference of the incident and scattered fields. The influence of spatial aliasing artifacts and amplitude errors on the spatial structure of the synthesized sound field are examined by numerical simulations.
Keywords: wave field synthesis, virtual scattering object, sound obstruction, equivalent source method

1. Introduction

Sound field synthesis is a physically-motivated approach for the reproduction of a desired sound field within an extended listening area. Typically, a dense arrangement of loudspeakers (termed secondary sources) is used in order to achieve a high spatial accuracy. The secondary sources are driven in such a way that the superposition of the individual sound fields is as similar as possible to the desired field. Among others, wave field synthesis (WFS) [1, 2] and near-field compensated higher-order Ambisonics (NFC-HOA) [3, 4] are the best known analytic approaches for sound field synthesis.

In order to synthesize a complex auditory scene, not only the sound waves emitted by virtual sources but also their interaction with virtual surfaces and objects have to be taken into account. While room reflections modify the sound field in a similar manner throughout the enclosed space, the scattering by an object causes a disturbance within a local area. One of the perceptually relevant phenomena in scattering is the acoustic shadow created behind the object. The higher the frequency, the more acoustic energy is obstructed by the scatterer. This leads to a low-pass filtered spectrum in the acoustic shadow. This spectral cue enables one to detect the existence of a silent object without any other sensory information [5, 6, 7, 8]. This is of particular interest in understanding the ability of visually impaired individuals to navigate relying solely on auditory cues [9]. Therefore, synthesizing a sound field including scattering objects can be used not only in applications for entertainment [10], but also for the design of a training system to enhance the echolocation ability [11, 12].

The aim of this paper is to synthesize a virtual sound field including a scattering object by using WFS. In Sec. 2, the incident field and the scattered field are represented in terms of spherical harmonics. The 2.5D WFS driving function is introduced in Sec. 3. The proposed driving function is used to

synthesize the desired sound field in Sec. 4, and the spatial and spectral properties of the synthesized sound fields are examined.

Nomenclature The following notational conventions are used throughout this paper. A sound field in the temporal frequency domain is denoted by uppercase $S(\mathbf{x}, \omega)$ where $\mathbf{x}$ denotes a position vector. The angular frequency ω is related to the temporal frequency f by $\omega = 2\pi f$. The spherical coordinate representation (r, θ, ϕ) is related to the Cartesian coordinate as $x = r\sin\theta\cos\phi, y = r\sin\theta\sin\phi, z = r\cos\theta$. The speed of sound is denoted by c, and the imaginary unit is denoted by i.

2. Scattering of a Sound Field

2.1 Spherical harmonics representation

A sound field scattered by an object is represented as a superposition of the incident field and the scattered field, $S(\mathbf{x}, \omega) = S_\mathrm{i}(\mathbf{x}, \omega) + S_\mathrm{s}(\mathbf{x}, \omega)$. For a given expansion center $\mathbf{x}_c$, the sound field can be expanded in terms of spherical harmonics. In a source-free region, the incident field is represented as an interior expansion [13, Sec. 6.8]

$$S_\mathrm{i}(\mathbf{x}, \omega) = \sum_{n=0}^{\infty} \sum_{m=-n}^{n} \breve{S}_n^m(\omega) j_n(\tfrac{\omega}{c} r) Y_n^m(\theta, \phi), \tag{1}$$

where $\breve{S}_n^m(\omega)$ denotes the expansion coefficient, $j_n(\frac{\omega}{c} r)$ the n-th order spherical Bessel function of the first kind, and $Y_n^m(\theta, \phi)$ the spherical harmonic of degree n and order m. The spherical harmonic is defined as [13, Sec. 6.3.3]

$$Y_n^m(\theta, \phi) = \sqrt{\frac{2n+1}{4\pi} \frac{(n-m)!}{(n+m)!}} P_n^m(\cos\theta) e^{im\phi}, \tag{2}$$

with $P_n^m(\cdot)$ denoting the associated Legendre function. The spherical coordinates are defined as $\mathbf{x} - \mathbf{x}_c = (r, \theta, \phi)$. For a compact scattering object bounded within a volume ($\|\mathbf{x} - \mathbf{x}_c\| \leq R$), the scattered sound field is given as an exterior expansion [14, Sec. 2.4.3]

$$S_\mathrm{s}(\mathbf{x}, \omega) = \sum_{n=0}^{\infty} \sum_{m=-n}^{n} \breve{A}_n^m(\omega) h_n^{(2)}(\tfrac{\omega}{c} r) Y_n^m(\theta, \phi), \tag{3}$$

where $\breve{A}_n^m(\omega)$ denotes the expansion coefficient, and $h_n^{(2)}(\frac{\omega}{c} r)$ the n-th order spherical Hankel function of the second kind.

2.2 Boundary conditions

The expansion coefficient of the scattered field is determined by the boundary condition imposed on the surface of the scatterer. In the following, a spherical scatterer with radius a centered at $\mathbf{x}_c$ is assumed, as illustrated in Fig. 1(a). The boundary condition on the spherical surface $\|\mathbf{x} - \mathbf{x}_c\| = a$ reads [15, Eq. (4.2.2)]

$$\frac{\partial S(\mathbf{x}, \omega)}{\partial r} + \frac{i}{\mathcal{Z}} S(\mathbf{x}, \omega) = 0, \tag{4}$$

where $\mathcal{Z}$ denotes the acoustic impedance at the surface. The expansion coefficient of the scattered field thus reads [15, Eq. (4.2.9)]

$$\breve{A}_n^m(\omega) = -\frac{\frac{\omega}{c} j_n'(\frac{\omega}{c} a) + \frac{1}{\mathcal{Z}} j_n(\frac{\omega}{c} a)}{\frac{\omega}{c} h_n^{(2)\prime}(\frac{\omega}{c} a) + \frac{1}{\mathcal{Z}} h_n^{(2)}(\frac{\omega}{c} a)} \breve{S}_n^m(\omega). \tag{5}$$

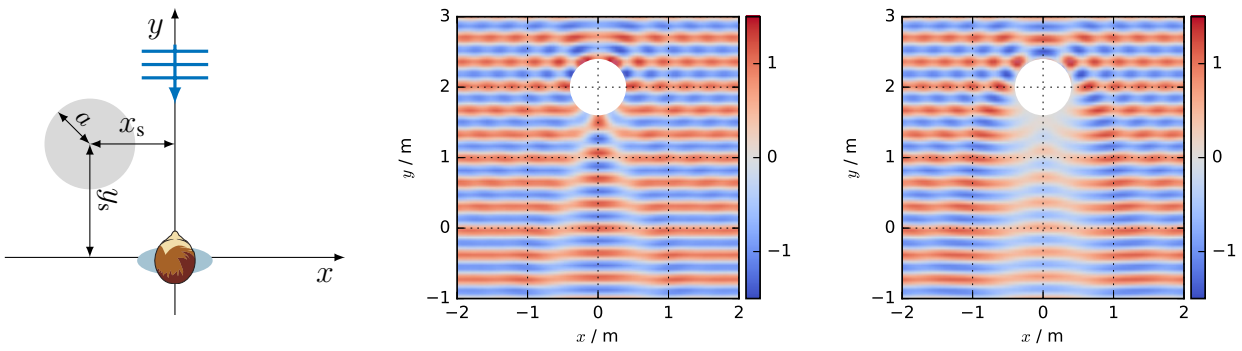

(a) Configuration (b) Sound-hard (c) Sound-soft

Figure 1: Sound field of a plane wave ($\phi_{\text{pw}} = -\frac{\pi}{2}$) scattered by a sphere of radius a centered at $(x_\text{s}, y_\text{s}, 0)$. Monochromatic ($f = 1$ kHz) examples are shown for (b) sound-hard and (c) sound-soft scatterers where $x_\text{s} = 0, y_\text{s} = 2$, and $a = 0.4$ m

For a sound-hard (rigid) scatterer, $\mathcal{Z}$ tends to infinity and (4) constitutes a Neumann boundary condition which specifies the derivative of the sound pressure field. The radial component of the particle velocity thus vanishes at the surface of the sphere, and the expansion coefficient of the scattered field reads

$$\breve{A}_n^m(\omega) = -\frac{j_n'(\frac{\omega}{c}a)}{h_n^{(2)'}(\frac{\omega}{c}a)}\breve{S}_n^m(\omega). \tag{6}$$

For a sound-soft (pressure release) scatterer, where $\mathcal{Z}=0$, (4) constitutes a Dirichlet boundary condition which specifies the sound pressure along the surface. The coefficient of the scattered field reads

$$\breve{A}_n^m(\omega) = -\frac{j_n(\frac{\omega}{c}a)}{h_n^{(2)}(\frac{\omega}{c}a)}\breve{S}_n^m(\omega). \tag{7}$$

The superposition of $S_\text{i}(\mathbf{x}, \omega)$ and $S_\text{s}(\mathbf{x}, \omega)$ is represented as a combination of an interior expansion and an exterior expansion [13, Sec. 6.10],

$$S(\mathbf{x}, \omega) = \sum_{n=-\infty}^{\infty} \sum_{m=-n}^{n} \left(\breve{S}_n^m(\omega) j_n(\tfrac{\omega}{c}r) + \breve{A}_n^m(\omega) h_n^{(2)}(\tfrac{\omega}{c}r) \right) Y_n^m(\theta, \phi), \tag{8}$$

where either (6) or (7) is plugged into (3) and added to (1).

In practice, the spherical harmonic expansion (8) can be only approximated by a finite number of terms. The maximum harmonic order N is termed as the modal bandwidth of a truncated expansion. The modal truncation error for interior and exterior expansions is investigated in [16] and [15, Ch. 9], respectively. Although $\breve{A}_n^m(\omega)$ is computed from $\breve{S}_n^m(\omega)$, this does not mean that the total sound field $S(\mathbf{x}, \omega)$ has to be represented with the same coefficients. For instance, the modal bandwidth of $S_\text{i}(\mathbf{x}, \omega)$ can be different from the modal bandwidth of $S_\text{s}(\mathbf{x}, \omega)$. Furthermore, $S_\text{i}(\mathbf{x}, \omega)$ can be expanded with respect to a new expansion center $\mathbf{x}_t$,

$$S(\mathbf{x}, \omega) = \underbrace{\sum_{n=\nu}^{N_\text{i}} \sum_{\mu=-\nu}^{\nu} \breve{S}_\nu^\mu(\omega) j_\nu(\tfrac{\omega}{c}r') Y_\nu^\mu(\theta', \phi')}_{S_\text{i}(\mathbf{x},\omega)} + \underbrace{\sum_{n=0}^{N_\text{s}} \sum_{m=-n}^{n} \breve{A}_n^m(\omega) h_n^{(2)}(\tfrac{\omega}{c}r) Y_n^m(\theta, \phi)}_{S_\text{s}(\mathbf{x},\omega)}, \tag{9}$$

where $\breve{S}_\nu^\mu(\omega)$ denotes the coefficient of the translated spherical harmonics expansion. The primed variables are defined as $\|\mathbf{x} - \mathbf{x}_t\| = (r', \theta', \phi')$. N_i and N_s denote the modal bandwidths of $S_\text{i}(\mathbf{x}, \omega)$ and $S_\text{s}(\mathbf{x}, \omega)$, respectively.

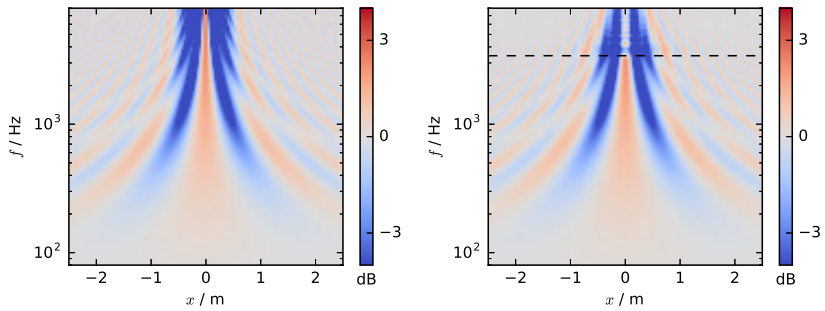

(a) Sound-hard ($N_\mathrm{s} = 75$)

(b) Sound-hard ($N_\mathrm{s} = 25$)

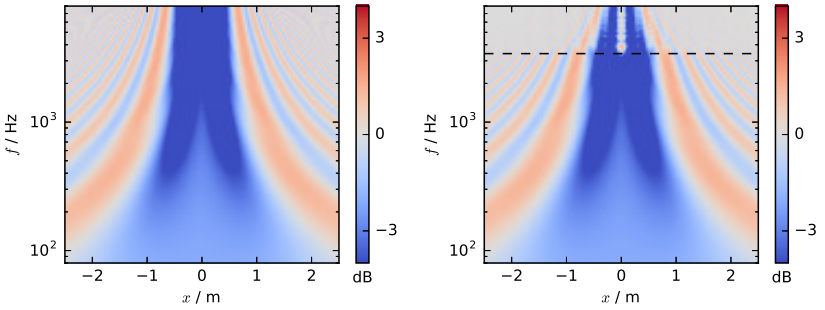

(c) Sound-soft ($N_\mathrm{s} = 75$)

(d) Sound-soft ($N_\mathrm{s} = 25$)

Figure 2: Frequency responses of scattered sound fields. An incident plane wave ($\phi_\mathrm{pw} = -\frac{\pi}{2}$) is scattered by a sphere of radius 0.4 m at $(0, 2, 0)$. The evaluation point is varied on the x-axis between -1.5 and 1.5 m. A modal band-limitation is applied only to $S_\mathrm{s}(\mathbf{x}, \omega)$. The truncation errors occur above the frequency $f_N = \frac{cN}{2\pi a}$ indicated by dashed lines in (c) and (d) ($f_{25} \approx 3.4$ kHz). The colormaps are clipped to ± 4 dB.

2.3 Spatial and Spectral Properties

In this section, an incident plane wave is considered which propagates parallel to the xy-plane ($\theta_\mathrm{pw} = \frac{\pi}{2}$) with polar angle ϕ_pw

$$S_\mathrm{i}(\mathbf{x}, \omega) = e^{-i\frac{\omega}{c} r \cos(\phi - \phi_\mathrm{pw})}, \tag{10}$$

as illustrated in Fig. 1(a). The expansion coefficient for the plane wave reads [13, Eq. (6.175)]

$$S_\mathrm{i}(\mathbf{x}, \omega) = 4\pi i^{-n} j_n(\tfrac{\omega}{c} r) Y_n^m(\tfrac{\pi}{2}, \phi_\mathrm{pw})^*, \tag{11}$$

where $(\cdot)^*$ denotes the complex conjugate. The resulting sound fields for sound-hard and sound-soft scatterers are shown in Fig. 1(b) and 1(c), respectively. The frequency responses are shown in Fig. 2 for different receiver positions. As can be seen in Fig. 1(b) and 1(c), the most apparent difference between the two boundary conditions is the shape and size of the acoustic shadow behind the sphere. For the sound-hard scatterer, a high amplitude is observed right in the middle of the acoustic shadow, which is due to the constructive interferences of the diffracted waves. For lower frequencies (< 200 Hz), a slight boost is observed for the sound-hard scatterer (Fig. 2(a)) whereas a slight attenuation can be seen for the sound-soft scatterer (Fig. 2(c)). The acoustic shadow of the sound-soft scatterer is wider and its width is more uniform. Fig. 2(b) and 2(d) show that a modal truncation causes deviations at higher frequencies, the lower bound of which can be approximated as $f_N = \frac{cN}{2\pi a}$. Interestingly, the erroneous magnitude responses above f_N seem similar for sound-hard and sound-soft cases.

3. Wave Field Synthesis

Assuming the secondary source distribution to be continuous, the sound field synthesis problem can be formulated as an integral equation

$$S(\mathbf{x},\omega) = \int_{\partial\Omega_0} D(\mathbf{x}_0,\omega) G(\mathbf{x}-\mathbf{x}_0,\omega) \mathrm{d}A_0, \tag{12}$$

where $G(\mathbf{x}-\mathbf{x}_0,\omega)$ denotes the Green's function of the secondary source at $\mathbf{x}_0 = (r_0,\theta_0,\phi_0) \in \partial\Omega_0$, $D(\mathbf{x}_0,\omega)$ the corresponding driving function, and $\mathrm{d}A_0$ the surface element.

Instead of solving (12) directly, the WFS driving function is derived by introducing a high-frequency/far-field approximation to the Kirchhoff-Helmholtz integral equation and assuming a Neumann boundary condition [17, Ch. 2]. This eliminates the dipole term of the Kirchhoff-Helmholtz integral which is simplified to a form as (12). The spectral weight of the remaining monopole term is interpreted as the WFS driving function, which is given as the directional gradient of $S(\mathbf{x},\omega)$ with respect to the normal vector $\mathbf{n}(\mathbf{x}_0)$ [2, Sec. 2],

$$D(\mathbf{x}_0,\omega) = -2a(\mathbf{x}_0) \langle \nabla S(\mathbf{x},\omega)|_{\mathbf{x}=\mathbf{x}_0}, \mathbf{n}(\mathbf{x}_0) \rangle, \tag{13}$$

where $\nabla S(\mathbf{x},\omega)|_{\mathbf{x}=\mathbf{x}_0}$ denotes the gradient of the sound field evaluated at the respective secondary source position, and $\langle \cdot,\cdot \rangle$ the inner product of two vectors. The secondary source selection window $a(\mathbf{x}_0)$ ensures that the propagation direction of the synthesized sound field is correct [18]. For a comprehensive overview of WFS, the reader is refer to [2, 17].

In this paper, a 2.5D configuration is considered where a two-dimensional sound field is synthesized only in the xy-plane by using a secondary point sources distributed on the same plane. Due to the dimensionality mismatch between the desired sound field (2D) and the acoustic properties of the secondary sources (3D), amplitude deviations occur in the synthesized sound field [19, 20]. In practice, the continuous distribution of the secondary sources is discretized and only a finite number of secondary sources are used. This constitutes a spatial sampling of the driving function which results in spatial aliasing artifacts [21].

Since the desired sound field is represented with spherical harmonics, the directional gradient has to be evaluated in the spherical coordinate system and the driving function is given as a series expansion. The WFS driving function based on circular/spherical harmonics representations are introduced in [22, 23, 24, 25]. According to [25, Eq. (27)], the 2.5D WFS driving function for the scattered field reads

$$\begin{aligned} D_\mathrm{s}(\mathbf{x},\omega) = &- 2a(\mathbf{x}_0) \sqrt{\tfrac{2\pi\|\mathbf{x}_\mathrm{ref}-\mathbf{x}_0\|}{i\frac{\omega}{c}}} \sum_{m=-N_\mathrm{s}}^{N_\mathrm{s}} \frac{\breve{A}^m_{|m|}}{4\pi i^{m-|m|} Y_m^{-|m|}(\frac{\pi}{2},0)} \\ &\times \left[\langle \hat{\mathbf{e}}_r, \mathbf{n}(\mathbf{x}_0) \rangle \tfrac{\omega}{2c} \left(H^{(2)}_{m-1}(\tfrac{\omega}{c} r_0) - H^{(2)}_{m+1}(\tfrac{\omega}{c} r_0) \right) + \langle \hat{\mathbf{e}}_\phi, \mathbf{n}(\mathbf{x}_0) \rangle (im) H^{(2)}_m(\tfrac{\omega}{c} r_0) \right] e^{im\phi_0}, \end{aligned} \tag{14}$$

where $H^{(2)}_m(\cdot)$ denotes the m-th order Hankel function of the second kind, and $\hat{\mathbf{e}}_r$ and $\hat{\mathbf{e}}_\phi$ the respective unit vectors. Note that, due to the 2.5D configuration, only a subset of the expansion coefficients $\breve{A}^m_n(\omega)$ are required ($n = |m|$). The term $\sqrt{\|\mathbf{x}_\mathrm{ref}-\mathbf{x}_0\|}$ corrects the amplitude for the reference point $\mathbf{x}_\mathrm{ref}$. The driving function for the incident field can be computed similarly [25, Eq. (27)]

$$\begin{aligned} D_\mathrm{i}(\mathbf{x},\omega) = &- 2a(\mathbf{x}_0) \sqrt{\tfrac{2\pi\|\mathbf{x}_\mathrm{ref}-\mathbf{x}_0\|}{i\frac{\omega}{c}}} \sum_{m=-N_\mathrm{i}}^{N_\mathrm{i}} \frac{\breve{S}^m_{|m|}}{4\pi i^{m-|m|} Y_m^{-|m|}(\frac{\pi}{2},0)} \\ &\times \left[\langle \hat{\mathbf{e}}_r, \mathbf{n}(\mathbf{x}_0) \rangle \tfrac{\omega}{2c} \left(J_{m-1}(\tfrac{\omega}{c} r_0) - J_{m+1}(\tfrac{\omega}{c} r_0) \right) + \langle \hat{\mathbf{e}}_\phi, \mathbf{n}(\mathbf{x}_0) \rangle (im) J_m(\tfrac{\omega}{c} r_0) \right] e^{im\phi_0}, \end{aligned} \tag{15}$$

where $J_m(\cdot)$ denotes the m-th order Bessel function of the first kind. The expansion center of (15) has to be chosen carefully. A modally band-limited interior expansion exhibits a high accuracy only

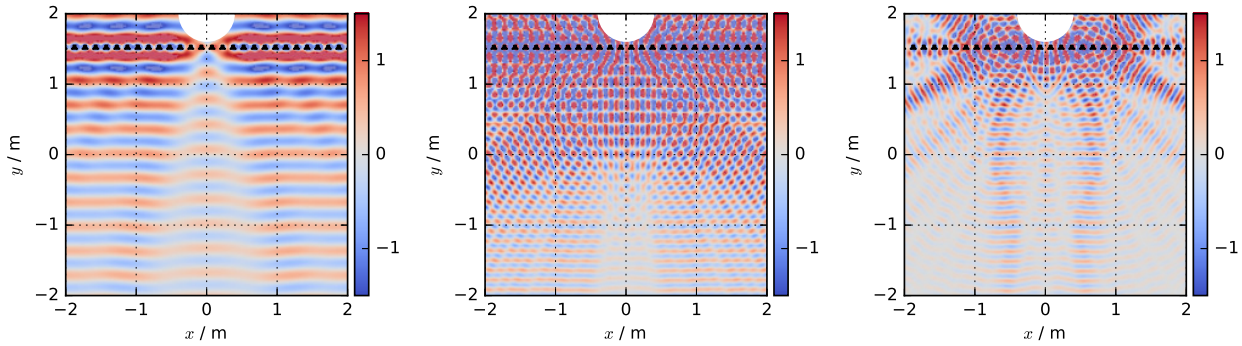

(a) $f = 1$ kHz (b) $f = 2.5$ kHz (c) $f = 2.5$ kHz, $N_\mathrm{i} = 15$

Figure 3: Monochromatic sound fields synthesized using 60 loudspeakers uniformly distributed on the line $y = 1.5$ m with spacing of $\Delta x = 0.15$ m. An incident plane wave ($\phi_\mathrm{pw} = -\frac{\pi}{2}$) is scattered by a rigid ($\mathcal{Z} = \infty$) sphere with radius of $a = 0.4$ m placed at $(0, 2, 0)$. In (a) and (b), a modal truncation ($N_\mathrm{s} = 15$) is applied only on $S_\mathrm{s}(\mathbf{x}, \omega)$, while in (c), the same modal truncation is applied on both $S_\mathrm{i}(\mathbf{x}, \omega)$ and $S_\mathrm{s}(\mathbf{x}, \omega)$.

within a circular/spherical region in the vicinity of the expansion center [16]. It is thus beneficial to expand the incident field with respect to a point in the middle of the listening area. If the incident field is a plane wave or a spherical wave, the analytic driving functions introduced in [2, Eq. (27) and (29)] can be used, which exhibit infinite modal bandwidths.

4. Evaluation

In this section, the proposed driving function is used for the synthesis of a sound field including a scattering sphere. Again, the configuration in Fig. 1(a) is considered. The sound field is synthesized by using 60 secondary monopole sources distributed on the line $y = 2$ m with spacing of $\Delta x = 0.15$ m. Figure 3 shows the synthesized sound field for a sound-hard sphere. In Fig. 3(a) and 3(b), a modal band-limitation was applied only to the driving function of the scattered field $D_\mathrm{s}(\mathbf{x}_0, \omega)$. The incident plane wave was synthesized by using the driving function in [2, Eq. (27)] which exhibits an infinite modal bandwidth. In Fig. 3(a), the interference of the incident and scattered field is appropriately synthesized, apart from amplitude deviations. For higher frequencies, shown in Fig. 3(b), the sound field is impaired due to spatial aliasing artifacts. The artifacts are mostly distributed in the upper part of the listening area. The higher the frequency, the more spatial aliasing occurs and the smaller gets the acoustic shadow. The influence of spatial aliasing for different frequencies is shown in Fig. 4. As can be seen in Fig. 4(a), the synthesized sound field suffers from spatial aliasing above the spatial aliasing frequency (≈ 2.3 kHz) irrespective of the listening position along the x-axis. Similar spectral responses are observed in Fig. 4(b) where the listener is fixed at $(0, 0, 0)$ and the position of the scattering sphere was varied. The deviations in the lower frequencies are attributed to the high-frequency approximation of the Kirchhoff-Helmholtz integral equation.

The spatial distribution of these artifacts can be controlled to some extent by applying a modal band-limitation to the incident field. In Fig. 3(c), the incident field is expanded at $(0, 0, 0)$ with a finite modal bandwidth ($N_\mathrm{i} = 15$). The desired sound field is synthesized more accurately within a circular area, but more deviations are observed outside. The local improvements in terms of spectral responses are demonstrated in Fig. 4(c) and Fig. 4(d). This approach is referred to as local WFS, where the position of the listener is assumed to be known and the synthesized sound field is optimized to the respective area [25].

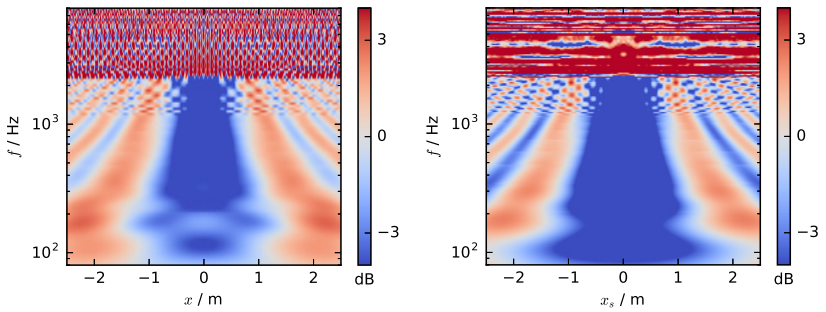

(a) $N_\mathrm{i} = \infty$, varying x

(b) $N_\mathrm{i} = \infty$, varying x_s

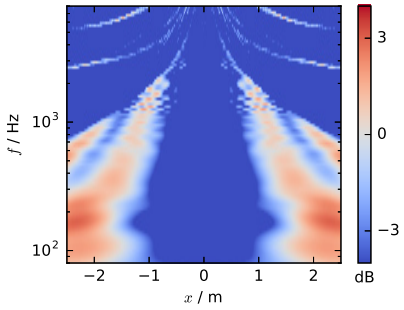

(c) $N_\mathrm{i} = 15$, varying x

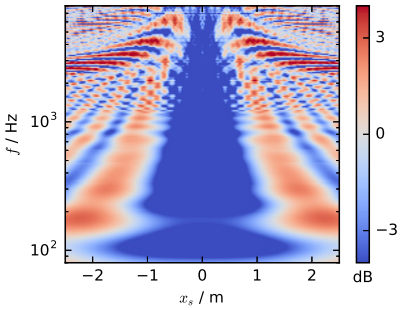

(d) $N_\mathrm{i} = 15$, varying x_s

Figure 4: Frequency responses of the synthesized sound fields. An incident plane wave ($\phi_\mathrm{pw} = -\frac{\pi}{2}$) is scattered by a sound-soft ($\mathcal{Z} = 0$) sphere or radius $a = 0.4$ m. The modal bandwidth of the driving function for $S_\mathrm{s}(\mathbf{x}, \omega)$ is truncated to $N = 15$. The driving function for $S_\mathrm{i}(\mathbf{x}, \omega)$ exhibits an infinite modal bandwidth in (a) and (b), and a finite modal bandwidth ($N = 15$) in (c) and (d). In (a) and (c), the listener position is varied on the line $y = 0$. In (b) and (d), the position of the scattering sphere is varied on $y = 2$. The colormaps are clipped to ± 4 dB.

5. Conclusion

In this paper, a virtual sound field was synthesized by WFS, where a virtual object scatters the incoming sound field. The scattered field is added to the incident field by synthesizing an equivalent source. The directivity of the source is determined by the boundary condition on the surface of the scatterer and represented by a spherical harmonics expansion. As a proof of concept, the sound field of a plane wave was synthesized which is scattered by a sphere. While the proposed approach performs properly at lower frequencies, spatial aliasing artifacts limit the performance at higher frequencies. In particular, the size of the acoustic shadow decreases above the spatial aliasing frequency. To overcome this problem, a modal band-limitation is applied to the incident field, which enables to control the position and size of the error-free region. The proposed method can be extended for more complex auditory scenes, e.g. multiple scatterers.

6. Acknowledgement

This research was supported by DFG SP 1295/7-1.

References

1. Berkhout, A. J., de Vries, D. and Vogel, P. Acoustic Control by Wave Field Synthesis, *The Journal of the Acoustical Society of America (JASA)*, **93** (5), 2764–2778, (1993).

2. Spors, S., Rabenstein, R. and Ahrens, J. The Theory of Wave Field Synthesis Revisited, *Proc. of 124th Audio Engineering Society (AES) Convention*, Amsterdam, The Netherlands, May, (2008).

3. Daniel, J. Spatial Sound Encoding Including Near Field Effect: Introducing Distance Coding Filters and a Viable, New Ambisonic Format, *Proc. of 23rd Audio Engineering Society (AES) International Conference on Signal Processing in Audio Recording and Reproduction*, Helsingør, Denmark, May, (2003).
4. Ahrens, J. and Spors, S. An Analytical Approach to Sound Field Reproduction using Circular and Spherical Loudspeaker Distributions, *Acta Acustica united with Acustica*, **94** (6), 988–999, (2008).
5. Supa, M., Cotzin, M. and Dallenbach, K. M. " Facial vision": The Perception of Obstacles by the Blind, *The American Journal of Psychology*, **57** (2), 133–183, (1944).
6. Gordon, M. S. and Rosenblum, L. D. Perception of Sound-obstructing Surfaces Using Body-scaled Judgments, *Ecological Psychology*, **16** (2), 87–113, (2004).
7. Dufour, F. Acoustic Shadows: An Auditory Exploration of the Sense of Space, *Sound Effects*, **1** (1), 82–97, (2011).
8. Miura, T., Ifukube, T. and Furukawa, S. Contribution of Acoustical Characteristics to Auditory Perception of Silent Object, *IEEE International Conference on Systems, Man, and Cybernetics (SMC)*, Anchorage, AK, USA, Oct., (2011).
9. Schenkman, B. N. and Nilsson, M. E. Human Echolocation: Blind and Sighted Persons' Ability to Detect Sounds Recorded in the Presence of a Reflecting Object, *Perception*, **39** (4), 483–501, (2010).
10. Mehra, R., Raghuvanshi, N., Antani, L., Chandak, A., Curtis, S. and Manocha, D. Wave-based Sound Propagation in Large Open Scenes Using an Equivalent Source Formulation, *ACM Transactions on Graphics (TOG)*, **32** (2), 19, (2013).
11. Spagnol, S., Johannesson, O. I., Kristjansson, A., Unnthorsson, R., Saitis, C., Kalimeri, K., Bujacz, M. and Moldoveanu, A. Model-based Obstacle Sonification for the Navigation of Visually Impaired Persons, *Proc. 19th International Conference on Digital Audio Effects (DAFx)*, Brno, Czech Republic, Sep., (2016).
12. Seki, Y. and Sato, T. A Training System of Orientation and Mobility for Blind People Using Acoustic Virtual Reality, *IEEE Transactions on neural systems and rehabilitation engineering*, **19** (1), 95–104, (2011).
13. Williams, E. G., *Fourier Acoustics: Sound Radiation and Nearfield Acoustical Holography*, Academic press (1999).
14. Teutsch, H., *Modal Array Signal Processing: Principles and Applications of Acoustic Wavefield Decomposition*, vol. 348, Springer Science & Business Media (2007).
15. Gumerov, N. A. and Duraiswami, R., *Fast Multipole Methods for the Helmholtz Equation in Three Dimensions*, Elsevier (2005).
16. Kennedy, R. A., Sadeghi, P., Abhayapala, T. D. and Jones, H. M. Intrinsic Limits of Dimensionality and Richness in Random Multipath Fields, *IEEE Transactions on Signal Processing*, **55** (6), 2542–2556, (2007).
17. Schultz, F., *Sound Field Synthesis for Line Source Array Applications in Large-Scale Sound Reinforcement*, Ph.D. thesis, University of Rostock, (2016).
18. Spors, S. Extension of an Analytic Secondary Source Selection Criterion for Wave Field Synthesis, *Proc. of 123rd Audio Engineering Society (AES) Convention*, New York, USA, Oct., (2007).
19. Variable Acoustics by Wavefield Synthesis: A Closer Look at Amplitude Effects, author=Sonke, Jan-Jakob and Labeeuw, Joeri and de Vries, Diemer, booktitle=Proc. of 104th Audio Engineering Society (AES) Convention, year=1998, month = may, address= Amsterdam, The Netherlands, organization=Audio Engineering Society.
20. Spors, S., Renk, M. and Rabenstein, R. Limiting Effects of Active Room Compensation using Wave Field Synthesis, *Proc. of 118th Audio Engineering Society (AES) Convention*, Barcelona, Spain, May, (2005).
21. Spors, S. and Rabenstein, R. Spatial Aliasing Artifacts Produced by Linear and Circular Loudspeaker Arrays used for Wave Field Synthesis, *120th Convention of the Audio Engineering Society*, Paris, France, May, (2006).
22. Corteel, E. Synthesis of Directional Sources Using Wave Field Synthesis, Possibilities, and Limitations, *EURASIP Journal on Advances in Signal Processing*, **2007** (1), 1–18, (2007).
23. Fazi, F. M., Olivieri, F., Carpentier, T. and Noisternig, M. Wave Field Synthesis of Virtual Sound Sources with Axisymmetric Radiation Pattern Using a Planar Loudspeaker Array, *Proc. of 134th Audio Engineering Society (AES) Convention*, Rome, Italy, May, (2013).
24. Ahrens, J. and Spors, S. Implementation of Directional Sources in Wave Field Synthesis, *IEEE Workshop on Applications of Signal Processing to Audio and Acoustics (WASPAA)*, New Paltz, USA, Oct., (2007).
25. Hahn, N., Winter, F. and Spors, S. Local Wave Field Synthesis by Spatial Band-limitation in the Circular/Spherical Harmonics Domain, *Proc. of 140th Audio Engineering Society (AES) Convention*, Paris, France, Jun., (2016).